Coherent $\pi^0\eta$ photoproduction on s-shell nuclei

M. Egorov and A. Fix[*]

Laboratory of Mathematical Physics, Tomsk Polytechnic University, 634050 Tomsk, Russia

(Received 29 May 2013; revised manuscript received 15 October 2013; published 18 November 2013)

Coherent photoproduction of $\pi^0\eta$ on the deuteron and ^{3}He and ^{4}He nuclei is considered in the energy region from threshold to a laboratory photon energy $E_\gamma = 1.2$ GeV. The transition amplitude is derived in the impulse approximation. The effects of pion absorption are included by means of the Fernbach-Serber-Taylor model. For the reactions on d and ^{3}He the interaction of the produced η meson with the recoiling nucleus is taken into account. The corresponding ηd and η^3He scattering amplitudes are obtained as solutions of the few-body equations for ηNN and $\eta - 3N$ systems. The impact of this interaction on the differential cross section in the region of small relative η-nuclear momenta is discussed.

DOI: 10.1103/PhysRevC.88.054611 PACS number(s): 25.20.Lj, 13.60.Le, 14.20.Gk

I. INTRODUCTION

Among different photoproduction channels special interest is focused today on the processes with two pseudoscalar mesons in the final state. The experimental study of $\pi\pi$ and $\pi\eta$ photoproduction on nucleons and nuclei have become an important part of the research programs of the European Laboratory for Structural Assessment (ELSA) and the Mainz Microtron (MAMI) facilities [1]. In particular, the database for $\pi^0\eta$ photoproduction was greatly extended by new very precise measurements, covering a large region of laboratory photon energies from threshold up to 3 GeV [2–5]. Furthermore, a considerable amount of new data for polarization observables has been reported in Refs. [6–9].

These new experimental results have generated a revival of theoretical interest in $\pi^0\eta$ photoproduction. Besides the most early studies of [10] a recent, rather detailed investigation of this process on a free proton was performed in Refs. [11–13]. Most of the efforts were directed toward understanding the general dynamical properties of those N^* and Δ resonances which are not very well seen in the reactions with a single meson and for which only weak evidence exists [14]. The analysis of the existing data within different models has provided further insights into the details of the nucleon excitation spectrum, in particular, in the third and the fourth resonance region.

It is however clear that a systematic study of meson photoproduction requires detailed information on the same process in nuclei. Here coherent reactions are of special use. Different studies clearly demonstrate their importance, especially in those cases for which the production proceeds dominantly via resonance excitations. One of the main motivations for studying these reactions is to obtain information on the isotopic structure of the elementary production amplitude. An evident advantage of using light nuclei as targets is the small number of nucleons. This allows one to minimize the influence of a nuclear environment on the elementary process on the one hand and to adopt an accurate microscopic description of the nuclear states on the other hand.

An important question related to $\pi^0\eta$ photoproduction on nuclei concerns the η-nuclear interaction in the final state. Although the η-nuclear scattering problem is by itself rather many-sided, the major related questions are connected to the one central point $-\eta N$ phenomenology in the low-energy regime. More specifically, the matter concerns the determination of the ηN low-energy interaction parameters, primarily the scattering length $a_{\eta N}$. In the absence of direct scattering results, the final state interaction (FSI) in the η production on nuclei remains the major source of information on ηN dynamics. A typical method of studying the ηN system in these reactions follows the scheme of (i) η production on nuclei, (ii) ηA model, and (iii) ηN interaction parameters. The central point in this sequence is the η-nuclear interaction model. Since in general one intends to connect ηA properties with those of ηN, the ηA model should be based on a refined microscopic approach, wherever possible, and at the same time, it should allow one to take systematically into account fundamental properties of the ηA system, such as unitarity of the scattering matrix, which is especially important at low energies.

The few-body calculations of Refs. [15–20], utilizing as a rule a separable ηN matrix, have already acquired the reputation of an effective theoretical method. Since these calculations are mostly restricted to systems with three and four particles, by now only η production on deuterium [21–25] and ^{3}He [26–28] have been considered in detail. According to the results of Refs. [20,26,28], for "reasonable" values of ηN scattering length with $\mathrm{Re}\,a_{\eta N} = 0.6 \pm 0.2$ fm and $\mathrm{Im}\,a_{\eta N} = 0.3 \pm 0.1$ fm, the ηN attraction is too weak to generate bound states of an η meson with two- and three-body nuclei, so that only virtual poles in the scattering matrices of these systems appear. On the other hand, for the higher values of $\mathrm{Re}a_{\eta N}$ of about 0.8–1.0 fm, the η-nuclear force becomes almost strong enough to bind the system. As a consequence, the corresponding virtual pole lies very close to the physical region, resulting in a strong enhancement of the η production cross section.

The case of ^{4}He is less clear. First, the existing data of [29] for the total cross section of $dd \to \eta^4$He show no threshold enhancement due to the final state interaction. Furthermore, for the same reaction in a recent experiment [30] no signal

[*]fix@mph.phtd.tpu.ru

from the decay of a hypothetical η-mesic ^{4}He into $\pi^- p\, ^3$He was detected. These results are rather surprising irrespective of the existence of η^4He bound states. They mean that the s-matrix pole, which in the case of η^3He seems to be close to the threshold energy on the Riemann surface, moves far away from this point when one turns to ^{4}He. Even if one takes into account a larger number of nucleons in ^{4}He and a substantial increase of its density, the total disappearance of a signal from the η^4He interaction in the measured spectrum is rather unexpected.

Second, there are still no correct few-body results for η^4He due to difficulty of the corresponding calculation. Less sophisticated theories, such as the optical model, are unable to take correctly into account important features of the low-energy η-nuclear interaction, for example, the importance of virtual target excitations between successive scattering events (see, e.g., [28]). Therefore, even the qualitative results obtained within this approach are unreliable. A further complication comes from the fact that it is the η^4He case where binding may appear. The value of the scattering length corresponding to a weakly bound or virtual state is known to be very sensitive to small variations of the potential parameters. Therefore, it may turn out that if we apply the few-body formalism to η^4He, the result will strongly depend not only on the ηN parameters but also on the approximations used to describe the structure of ^{4}He (e.g., on details of the NN forces at short distances, inclusion of a repulsive core into the NN potential, etc.). This may lead to a strong model dependence of the calculation, in addition to the five-body scattering problem being technically very difficult by itself.

Since no microscopic ηA calculations are available for nuclei with $A > 3$, methods allowing a model-independent extraction of the ηA scattering parameters directly from the measured observables are of special importance. Several steps have already been taken in Refs. [31–41], where information on the η-nuclear scattering from the characteristic behavior of the cross section in the region of small ηA relative energies was obtained. As a rule, the underlying method is based on the approach developed by Watson [42] and Migdal [43]. Under certain conditions this approach makes it possible to study the ηA interaction directly from a distribution over the relative ηA energy. The case in point is a characteristic enhancement of the η yield due to a strong attraction between the η meson and the recoiling nucleus. Here again, the coherent photoproduction of $\pi^0\eta$ seems to have some advantages over other reactions, such as $A(p,\eta p)A$ or $A(\pi,\eta N)B$, for which one has to take into account the interaction among all three final particles. Even the simplest case, when the composite nature of the nucleus is ignored (e.g., if one neglects its virtual excitations), requires a three-body calculation. This problem should be much less important for $\pi^0\eta$ photoproduction. In this case one can safely neglect the interaction between η and π^0, since in the energy region under discussion, $E_\gamma \leqslant 1.5$ GeV, this system does not resonate. As a result, the whole interaction process may be approximated by the sum of ηA and $\pi^0 A$ rescatterings.

Although the reactions $A(\gamma,\pi^0\eta)A$ offer important advantages, up to now rather little effort has been devoted to their theoretical study. Perhaps, the major reason for this is the difficulty of the experimental identification of these reactions due to the smallness of the coherent cross section in comparison to the background quasifree process $A(\gamma,\pi^0\eta N)$. This situation should change with new measurements of $\pi^0\eta$ photoproduction on nuclei [1]. In anticipation of the new data, we present here theoretical results for $\pi^0\eta$ photoproduction on s-shell nuclei, for which we have chosen as specific examples d, ^{3}He, and ^{4}He.

II. MODEL INGREDIENTS

We consider the process

$$\gamma(E_\gamma,\vec{k};\vec{\varepsilon}_\lambda) + A(E_A,\vec{Q}_A) \to \pi^0(\omega_\pi,\vec{q}_\pi) + \eta(\omega_\eta,\vec{q}_\eta) + A(E'_A,\vec{Q}'_A), \quad (1)$$

where the four-momenta of the participating particles are given in parentheses. For the calculations we choose the laboratory frame where the initial nucleus A is at rest ($Q_A = 0$). The circular polarization vector of the photon is denoted by $\vec{\varepsilon}_\lambda$ with $\lambda = \pm 1$.

One of the features of the reaction (1) is a rather high momentum transfer associated with a relatively large mass of the $\pi\eta$ system. This first results in a rather low cross section (of several hundred nanobarns) and, moreover, in a sensitivity of its magnitude to details of the nuclear wave function at short internuclear distances. At the same time, this sensitivity does not necessarily mean that a refined microscopic nuclear model is required for the calculation. Indeed, according to our general notion of coherent production, its basic mechanism, yielding the main part of the amplitude, is the impulse approximation (IA) accompanied by FSI effects. Within this model, the unpolarized cross section is mainly governed by the nuclear form factor. The latter is free from ambiguities of the nuclear structure and may well be described phenomenologically without resorting to complicated microscopic calculations. Furthermore, the interaction of pions with nuclei in the resonance region is mostly manifested in the attenuation of the pion wave function inside the nucleus, which is rather insensitive to structural details of the nuclear model. As for the η-nuclear interaction, which is one of the main objects of the present study, in the low-energy region it is mainly determined by the long-range part of the η-nuclear wave function and therefore should also weakly depend on the model which is used to describe the nuclear subsystem. Taking into account this observation, we use for the nuclear wave functions the phenomenological models, which reproduce the corresponding form factors up to the values of momentum transfer which are characteristic for $\pi\eta$ production in the second and third resonance regions. For the deuteron we take the wave function of the Bonn potential (full model) [44]. For the ^{3}He target the separable parametrization from [45] is employed, and for ^{4}He we adopt the Fourier transform of the r-space wave function from [46].

The elementary operator has the well-known form reflecting the general spin structure of photoproduction of pseudoscalar mesons on spin 1/2 fermions:

$$t = L_\lambda + i\vec{K}_\lambda \cdot \vec{\sigma}, \quad (2)$$

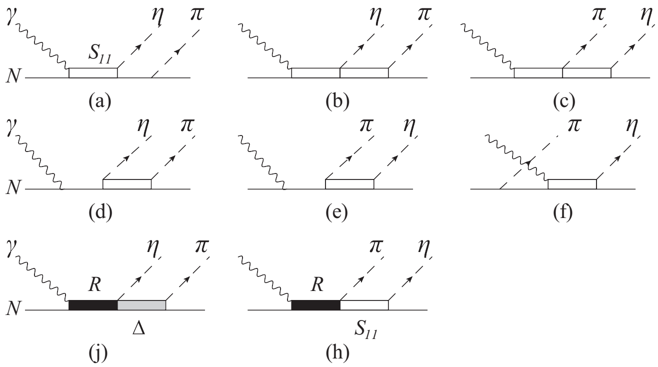

FIG. 1. Diagrams for the reaction $\gamma N \to \pi^0\eta N$ used in the present calculation. The isobars $\Delta(1232)$ and $S_{11}(1535)$ are denoted by Δ and S_{11}, respectively.

where $\lambda = \pm 1$ is the photon polarization index. In the case of the spin-zero nucleus ^{4}He the contribution of the spin-flip part $i\vec{K}_\lambda \cdot \vec{\sigma}$ vanishes exactly.

In order to calculate the amplitudes L_λ and $\vec{K}_\lambda$ we used the isobar model of Ref. [12] (first solution), which is based on the traditional phenomenological Lagrangian approach with Born and resonance contributions calculated on the tree level. The matrix element is diagrammatically illustrated in Fig. 1. It may be represented as a sum of a background amplitude and a resonance part:

$$t = t^B + \sum_{R(J^\pi, I)} t^R, \tag{3}$$

where the summation is performed over the resonance states R determined by their spin-parity J^π and isospin I.

The amplitude t^B contains the Born terms [diagrams (a)–(f) in Fig. 1] derived as a nonrelativistic reduction of the covariant photoproduction amplitudes keeping only terms up to the order (p/M_N), where M_N is the nucleon mass. Here we included only the most important Born diagrams, neglecting those containing the ηNN coupling as well as baryon resonances in the u channel.

The resonance part [diagrams (j) and (h) in Fig. 1] includes those baryon resonances which are localized in the mass region up to 1.95 GeV and have an appreciable $\pi\eta N$ decay width. Apart from the dominant $D_{33}(1700)$ and $D_{33}(1940)$ resonances, the model also contains the positive-parity states $P_{33}(1600)$, $P_{31}(1750)$, $F_{35}(1905)$, and $P_{33}(1920)$. The parameters of the resonances were fitted to the experimental angular distributions of π and η mesons in $\gamma p \to \pi^0\eta p$ as described in Ref. [12].

To take into account multiple scattering in the πN and ηN subsystems, the $\Delta(1232)$ and $S_{11}(1535)$ isobars were introduced. Then the final $\pi\eta N$ state results from a two-step decay via intermediate quasi-two-body channels $\eta\Delta$ and πS_{11}:

$$t^R = t^{R(\eta\Delta)} + t^{R(\pi S_{11})}, \tag{4}$$

as is schematically illustrated in Fig. 1.

In Fig. 2 we show the total cross section for $\gamma p \to \pi^0\eta p$. The contributions of different terms are separately presented on the right panel. According to the calculation, in the region up to $E_\gamma = 1.2$ GeV the major fraction of the cross section is provided by the resonance $D_{33}(1700)$.

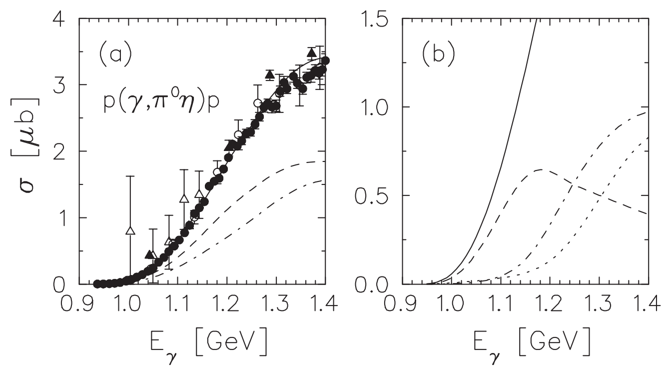

FIG. 2. Total cross section for $\gamma p \to \pi^0\eta p$ calculated using the isobar model of Ref. [12] (solid curve on both panels). On panel (a), the dash-dotted and the dashed curves correspond to the spin-flip part $\vec{K}$ and the spin-independent part L in Eq. (2). The data are from Ref. [2] (open triangles), [3] (open circles), [4] (filled triangles), and [5] (filled circles). On panel (b), the dashed and dash-dotted curves show the contribution from the resonances $D_{33}(1700)$ and $D_{33}(1940)$, respectively. The dotted curve is the combined contribution of the remaining resonances [$P_{33}(1600)$, $P_{31}(1750)$, $F_{35}(1905)$, and $P_{33}(1920)$] and the Born terms.

On the left panel of Fig. 2 we also plotted the components σ_K and σ_L of the cross section coming from the spin-flip and spin-independent part of the operator (2). Neglecting all terms apart from $D_{33}(1700)$ one obtains for the ratio of σ_K to σ_L

$$\frac{\sigma_K}{\sigma_L} = \frac{1}{2} + \frac{1}{2}\left(\frac{3-\sqrt{3}a}{1+\sqrt{3}a}\right)^2, \tag{5}$$

where a is the ratio of the 3/2 to 1/2 helicity amplitudes of the $D_{33}(1700)$ resonance:

$$a = A_{3/2}/A_{1/2}. \tag{6}$$

In the model of Ref. [12] this parameter changes from 0.9 to 1.1 in the energy region $E_\gamma \leqslant 1.2$ GeV, where the $D_{33}(1700)$ resonance dominates (see Fig. 6 in [12]). Therefore, at these photon energies the ratio (5) remains almost constant and is equal to 0.60 ± 0.04, so that the components σ_K and σ_L are comparable, as may also be seen from Fig. 2.

Within the impulse approximation the nuclear transition operator is taken as a sum of single-nucleon operators (2),

$$T = \sum_{i=1}^{A} t_i, \tag{7}$$

with A denoting the number of nucleons in the target. By taking into account antisymmetrization of the initial and final nuclear wave functions, the amplitude on a nucleus is proportional to that on a single nucleon, sandwiched between the nuclear ground states with the spin J:

$$T_{\lambda MM'} = A\langle \vec{q}_\eta, \vec{q}_\pi; JM'|t_1(\omega)|\vec{k}, \lambda; JM\rangle, \tag{8}$$

where the operator t_1 acts on the nucleon '1'. The quantity ω in (8) denotes the invariant γN energy for a nucleon on the mass shell. To take properly into account the Fermi motion effect, which should be important in the resonance region, we use the prescription of Refs. [47,48], in which the elementary operator is frozen at the average effective nucleon momentum in the laboratory system,

$$\vec{p}_i = \langle \vec{p}_i \rangle = -\frac{A-1}{2A}\,\vec{Q}, \tag{9}$$

where $\vec{Q} = \vec{k} - \vec{q}_\pi - \vec{q}_\eta$ is the momentum transferred to the nucleus and A is the nuclear mass number. This choice is compatible with the requirements of energy and momentum conservation together with the on-mass-shell conditions for the nucleon in both the initial and final states.

The unpolarized cross section of the reaction (1) is proportional to the square of the amplitude (8) averaged over the initial spin states:

$$\frac{d\sigma}{d\Omega_\pi d\omega_\pi d\Omega_\eta^*} = \frac{1}{(2\pi)^5}\frac{E'_A q_\pi q_\eta^*}{8E_\gamma \omega_{\eta A} W} \times \frac{1}{2(2J+1)}\sum_{\lambda M M'} |T_{\lambda M M'}|^2, \tag{10}$$

where the total ηA energy $\omega_{\eta A}$, the η momentum $\vec{q}_\eta^{\,*}$, and the corresponding solid angle Ω_η^* are calculated in the ηA center-of-mass (c.m.) frame.

Of primary importance for the coherent reaction is the relative contribution of the transitions with isospins $I = 1/2$ and $3/2$. Since η is an isoscalar particle, the isospin structure of the operator (2) is similar to that of single pion photoproduction. In particular, for $\pi^0\eta$ we have

$$t = A^{(0)}\tau_3 + \tfrac{1}{3}A^{(1/2)} + \tfrac{2}{3}A^{(3/2)}, \tag{11}$$

where τ_3 is the third component of the nucleon isospin operator $\vec{\tau}$. The amplitudes $A^{(1/2)}$ and $A^{(3/2)}$ in (11) are related to the final $\pi^0\eta N$ state with isospins $I = 1/2$ and $3/2$, respectively. The isoscalar amplitude $A^{(0)}$ leads only to states with isospin $1/2$. According to the analyses of [10–12], in the energy region $E_\gamma = 1$–1.4 GeV the process (2) is dominated by the excitation of Δ-like resonances, so that the role of the $A^{(0)}$ and $A^{(1/2)}$ components is small in the energy region considered. Therefore, the resulting elementary cross section is practically the same for proton and neutron targets. For reactions on nuclei this means that the effect of coherence is maximal and the cross section does not depend on the isospin of the target.

To take into account the interaction between the emitted pion and the final nucleus we used a simplified model in which this interaction is described in terms of a classical propagation of a pion in nuclear matter. In the resonance region the major influence of the nucleus is the attenuation of the pion beam due to absorption. Apart from true absorption on nucleon pairs, the inelastically scattered pions, which in fact contribute to the incoherent cross section, are also treated as if they are absorbed.

An additional interaction effect, which however should be less important in the energy region considered, comes from the modification of the pion wave number in a nuclear medium, which in particular results in changing the diffraction patterns which are characteristic for coherent pion photoproduction in the resonance region. Here we neglect the latter effect and take into account only the absorption of the produced pions using a simple prescription. Namely, the cross section is multiplied

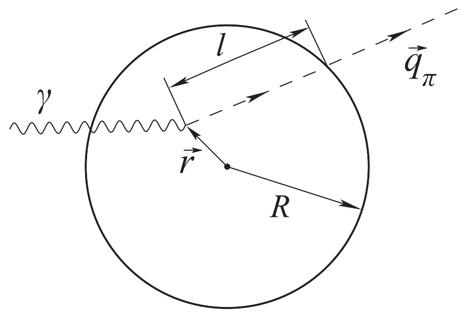

FIG. 3. Illustration of the distance $l(\vec{r}\,)$ in Eq. (13).

by an energy-dependent damping factor, which was calculated as follows. The pion wave function inside the nucleus was taken in the form used by Fernbach, Serber, and Taylor [49] for neutron interactions in nuclei:

$$\phi^{(-)}_{\vec{q}_\pi}(\vec{r}\,) = \exp(-i\vec{q}_\pi\cdot\vec{r}\,)D(\vec{r}\,), \tag{12}$$

where the damping factor

$$D(\vec{r}\,) = \exp[-l(\vec{r}\,)/2\lambda] \tag{13}$$

depends on the distance $l(\vec{r}\,)$, measured along the classical trajectory of a meson between the point where it was produced and the point where it escaped from the nucleus (see Fig. 3).

The optical properties of the nuclear environment are determined by the mean free path λ of a pion. The latter can be expressed (see, for example, Ref. [50]) through the depth of the imaginary part V_I of the square-well optical potential as

$$\lambda = -\frac{v}{2V_I}, \tag{14}$$

where v is the pion velocity in the rest frame of the nucleus. The values of V_I for nuclear matter were deduced in Ref. [50] from the pion-nucleon and pion-deuteron cross sections. In order to take into account the relatively low density of the deuteron, we multiplied V_I in Eq. (14) by the energy-independent factor

$$\xi = \frac{\rho_d}{\rho_{^4He}} \approx \frac{2/R_d^3}{4/R_{^4He}^3}, \tag{15}$$

where for R_d and $R_{^4He}$ the corresponding r.m.s. radii $R = \sqrt{\langle r^2\rangle}$ were used. The same procedure was applied to ^{3}He.

For simplicity we take the damping factor $D(\vec{r}\,)$ out of the matrix element at a mean value

$$\overline{D(\vec{r}\,)} = \frac{1}{A}\int_V D(\vec{r}\,)\rho(r)d^3r, \tag{16}$$

where V is the nuclear volume. For the nuclear density $\rho(r)$ in (14) and (16) a simple hard-sphere form

$$\begin{aligned}\rho(r) &= \frac{3A}{4\pi R^3}, \quad r < R,\\ &= \quad 0, \quad r > R,\end{aligned} \tag{17}$$

was taken.

The integral in Eq. (16) can quite easily be calculated in a cylindrical coordinate system. Choosing the origin of this system at the center of the nucleus and the z axis along the vector $\vec{q}_\pi$ one obtains for the distance $l(\vec{r}\,)$

$$l(\vec{r}\,) = \sqrt{R^2-\rho^2} - z, \tag{18}$$

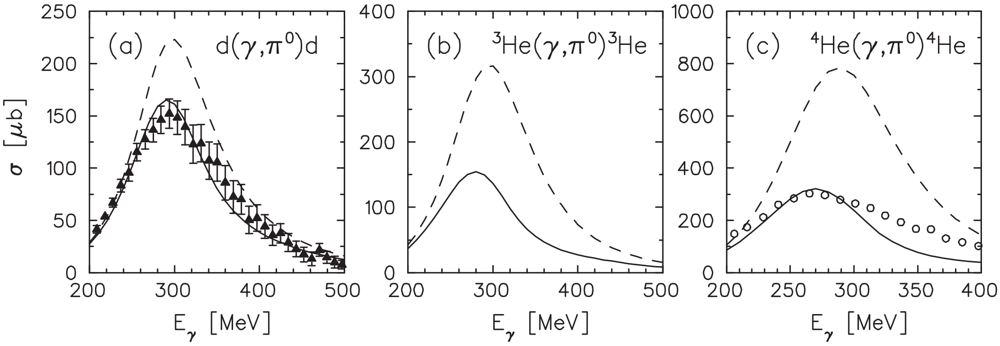

FIG. 4. Total cross section for coherent π^0 photoproduction on d, ^{3}He, and ^{4}He. The solid (dashed) curves are calculated using the impulse approximation with (without) pion absorption. The elementary $\gamma N \to \pi^0 N$ amplitude is taken from the MAID2007 model [52]. The data are from [53] (triangles) and [54] (circles).

where the polar radius and the height are denoted as ρ and z, respectively.

Using Eq. (18) in (13) and (16) one finds

$$\overline{D(\vec{r}\,)} = \frac{3}{2x}\left\{1 - \frac{2}{x^2}[1-(1+x)e^{-x}]\right\} \tag{19}$$

with

$$x = \frac{R}{\lambda}. \tag{20}$$

Then the absorption effect results in a suppression of the cross section by a factor $[\overline{D(\vec{r}\,)}]^2 \leqslant 1$ (see also Ref. [51]).

To demonstrate the quality of our treatment of the π-nuclear interaction in the final state, we show in Fig. 4 our results for coherent single π^0 photoproduction on all three nuclei in the first resonance region. As one can see, for the reaction on d and ^{4}He, the method provides the required suppression in the region of the maximum at $E_\gamma \approx 280$ MeV. Above $E_\gamma \approx 320$ MeV the calculated cross section underestimates the experimental results. However, in view of the extreme simplicity of our model the agreement may be regarded as quite reasonable.

In contrast to the pion case, the interaction in the η-nucleus system, where the major role is played by the strong s-wave attraction, is mostly important at lower relative energies. This well-known property is also observed in other reactions [32–36] where it leads to a pronounced peak in the distribution over the relative η-nuclear energy E in the region of small E values. To extract the ηA interaction parameters, one assumes that this FSI effect is independent of the η production mechanism and, therefore, can be unambiguously isolated. In fact, this assumption is justified only if the following conditions are fulfilled [42,43]: (i) the driving reaction mechanism ($\pi^0\eta$ photoproduction in our case) is of short-range nature, i.e., its effective radius is essentially smaller than the characteristic range of the ηA forces, and (ii) the attraction between the particles is comparatively strong and is characterized by a low relative momentum, so that it acts during a sufficiently long time. For the reactions with more than two strongly interacting particles in the final state a third obvious condition should be added: (iii) other particles having high velocities quickly escape the region in which the production mechanism works, and thus they have little effect on the interacting pair.

Of these three conditions the first two seem to be fairly well satisfied in our case. Indeed, the smallness of the effective range of an interaction responsible for $\pi\eta$ production is ensured by a rather large momentum transfer. The strong ηA attraction is due to a nearby pole in the corresponding s-wave amplitudes. The third condition is fulfilled due to the small pion mass, which results in a rather high velocity of the produced pion, so that in the major fraction of the reaction events it is at a distance well removed from the ηA pair. This latter aspect is considered in the next section in more detail.

Our method of calculating the η-nucleus final state interaction is very similar to that adopted for the reactions $\gamma d \to \eta d$ and $np \to \eta d$ in Refs. [19,23] as well as for ^{3}He$(\gamma,\eta)^3$He in Ref. [28]. It is based on the few-body scattering formalism with separable representation of the interactions in the ηN and NN subsystems. The latter were restricted to the s-wave states only, which are well known to strongly dominate the ηN and NN dynamics at low energies. Following Ref. [19], the subsystems ηN and NN will be denoted by N^* and d, respectively. For the corresponding scattering matrices we use the simplest rank-one separable ansatz. In detail, for the NN interaction in $^1S_0$ and $^3S_1$ states we take

$$t_d^{(s)}(z,q',q) = g_d^{(s)}(q')\tau_d^{(s)}(z)\,g_d^{(s)}(q), \tag{21}$$

where $s = 0, 1$ stand for the $^1S_0$ and $^3S_1$ NN states, respectively. The quasiparticle NN propagator reads

$$\tau_d^{(s)}(z) = -\frac{1}{2M_N}\left[1 - \frac{1}{4\pi^2}\int_0^\infty \frac{\left[g_d^{(s)}(q)\right]^2}{zM_N - q^2 + i\epsilon}\,q^2dq\right]^{-1}, \tag{22}$$

where M_N is the nucleon mass. For the vertex functions we used

$$g_d^{(s)}(q) = \sqrt{2}\pi\sum_{i=1}^{6}\frac{C_i^{(s)}}{q^2+\beta_i^{(s)2}}, \tag{23}$$

where the parameters $C_i^{(s)}$ and $\beta_i^{(s)}$ were fitted in Ref. [55] to the off-shell behavior of the Paris NN potential.

In the ηN state only the $S_{11}(1535)$ resonance, which provides the dominant contribution, was taken into account. To parametrize the corresponding ηN scattering matrix we

TABLE I. Parameters for ηd and η^3He low-energy scattering obtained within the few-body approach developed in Refs. [19] and [28]. For orientation the corresponding values of the ηN scattering length are also given.

	$a_{\eta N}$ (fm), Ref.	$a_{\eta d}$ (fm)	$r_{0\,\eta d}$ (fm)	a_{η^3He} (fm)	$r_{0\,\eta^3He}$ (fm)
1	$0.50 + i\,0.33$, [56]	$1.232 + i\,1.110$	$2.429 - i\,1.037$	$1.866 + i\,2.752$	$1.934 - i\,0.532$
2	$0.75 + i\,0.27$, [57]	$2.221 + i\,1.153$	$1.870 - i\,0.471$	$4.199 + i\,4.817$	$1.442 - i\,0.139$
3	$1.03 + i\,0.41$, [58]	$3.318 + i\,2.648$	$1.818 - i\,0.456$	$-3.767 + i\,9.362$	$1.631 - i\,0.187$

adopted an energy-dependent potential, leading to the familiar isobar ansatz

$$t_{N^*}(z, q', q) = g_{N^*}(q')\tau_{N^*}(z)g_{N^*}(q), \tag{24}$$

with

$$\tau_{N^*}(z) = \left[z - M_0 - \Sigma_\eta(z) - \Sigma_\pi(z) + \frac{i}{2}\Gamma_{\pi\pi}(z)\right]^{-1}, \tag{25}$$

where M_0 is the bare isobar mass and for $\alpha \in \{\eta, \pi\}$

$$\Sigma_\alpha(z) = \int_0^\infty \frac{\left[g^\alpha_{N^*}(q)\right]^2}{z - M_N - m_\alpha - q^2/2\mu_{\alpha N} + i\epsilon}\frac{q^2dq}{2\pi^2},$$
$$\text{with}\quad \mu_{\alpha N} = \frac{m_\alpha M_N}{m_\alpha + M_N}, \tag{26}$$

are the corresponding $S_{11}(1535)$ self-energies related to the ηN and πN channels. The two-pion channel was included in a simplified manner by adding the corresponding decay width $\Gamma_{\pi\pi}$, parametrized by

$$\Gamma_{\pi\pi}(z) = \gamma_{\pi\pi}\frac{z - M_N - 2m_\pi}{m_\pi}, \quad \gamma = 4.3\ \text{MeV}. \tag{27}$$

The ηN parameters were chosen in such a way that three different values of the ηN scattering length $a_{\eta N}$, listed in Table I, are reproduced and at the same time provide a reasonably good description of the reactions $\pi N \to \pi N$ and $\pi N \to \eta N$ in the S_{11} partial wave.

The separable representation of the driving two-particle potentials, as described above, allows one to reduce the n-body problem to a system of effective two-body equations of Lippmann-Schwinger type. In the three-body case ηNN the resulting equations read

$$X_{ij}(\vec p\,', \vec p\,) = Z_{ij}(\vec p\,', \vec p\,) + \sum_{k=1}^{3}\int \frac{d^3p''}{(2\pi)^3}Z_{ik}(\vec p\,', \vec p\,'')\tau_k X_{kj}(\vec p\,'', \vec p\,) \tag{28}$$

for $i, j = 1, 2, 3$ (where unessential spin-isospin indices are omitted) The amplitudes X_{ij} in (28) define the transitions between the quasi-two-body states $|i, \vec p\,\rangle$ containing the spectator particle i and the interacting two-particle subsystem (jk) (N^* or d). Denoting the nucleons as N_1 and N_2 we have three different states corresponding to three possible partitions of the ηNN system:

$$\begin{aligned}&(1): N_1 + (\eta N_2),\\ &(2): N_2 + (\eta N_1),\\ &(3): \eta + (N_1N_2).\end{aligned} \tag{29}$$

The relative momentum of particle i with respect to the center of mass of the other two particles (jk) is $\vec p$. The driving terms Z_{ij} $(i, j = 1, 2, 3)$ are the matrix elements of the free three-particle Green's function G_0:

$$Z_{ij}(\vec p\,', \vec p\,) = (1 - \delta_{ij})\langle i, \vec p\,'|G_0|j, \vec p\,\rangle. \tag{30}$$

As is shown in Ref. [19] the identity of nucleons allows one to reduce the set of equations (28) to only two independent equations, which may be presented in a schematic form as

$$X_{dd} = 2Z_{dN^*}\tau_{N^*}X_{N^*d}, \tag{31}$$
$$X_{N^*d} = Z_{N^*d} + Z_{N^*d}\tau_d X_{dd} + Z_{N^*N^*}\tau_{N^*}X_{N^*d}. \tag{32}$$

Their structure is illustrated in Fig. 5. The equations are similar to those obtained, e.g., in [59] for πNN scattering [see expressions (3.1) and (3.2) of this reference].

In Ref. [19], where coherent η photoproduction was studied, the incident η meson in the driving term Z_{N^*d} was simply replaced by the photon in order to take into account the electromagnetic interaction in the entrance channel:

$$Z_{dN^*} \to Z^{(\gamma)}_{dN^*} = \left\langle d, \vec k\left|G_0^{(\gamma)}\right|N^*(\gamma), \vec p\right\rangle, \tag{33}$$

where $G_0^{(\gamma)}$ is the free γNN propagator and $|N^*(\gamma)\rangle$ is the vertex function for the transition $\gamma N \to N^*$. Inserting Eq. (32) into Eq. (31) and making the substitution (33), one obtains the reaction amplitude in the form

$$X^{(\gamma)}_{dd} = V^{(\gamma)}_{dd} + V^{(\gamma)}_{dd}\tau_d X_{dd} + V^{(\gamma)}_{dN^*}\tau_{N^*}X_{N^*d}, \tag{34}$$

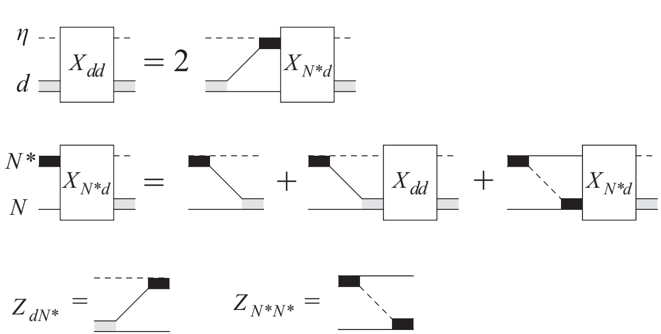

FIG. 5. Diagrammatic representation of the three-body integral equations (31) and (32).

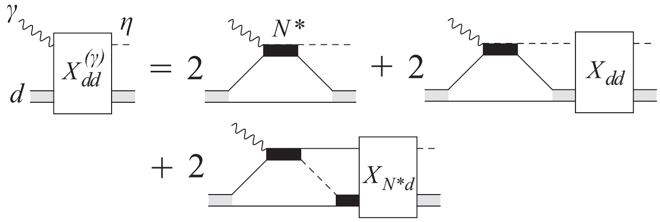

FIG. 6. Illustration of the amplitude (34) for coherent η photoproduction on a deuteron used in Ref. [19].

which is illustrated in Fig. 6. The effective driving terms in (34) are

$$V_{dd}^{(\gamma)} \equiv 2Z_{dN^*}^{(\gamma)}\tau_{N^*}Z_{N^*d}, \tag{35}$$

$$V_{dN^*}^{(\gamma)} \equiv 2Z_{dN^*}^{(\gamma)}\tau_{N^*}Z_{N^*N^*}. \tag{36}$$

Equations (31), (32), and (34) were used in Ref. [19] to calculate η photoproduction on a deuteron. In order to apply this formalism to the coherent photoproduction of $\pi^0\eta$ we simply replace the driving term $V_{dd}^{(\gamma)}$ in Eq. (34) by the amplitude T^{IA} for $d(\gamma,\pi^0\eta)d$ calculated in the impulse approximation. Since in this case the final state includes three free particles, the calculation of the integrated cross section becomes rather time consuming. For the sake of simplicity, we retained in the NN propagator τ_d only the pole contribution

$$\tau_d(z) \to \tau_d^0(z) = \frac{N_d^2}{z+|E_d|}, \tag{37}$$

where E_d is the deuteron binding energy and N_d is the normalization constant of the deuteron wave function. Furthermore, we dropped in (34) the less essential last term containing X_{N^*d} which leads to additional rescattering of the produced meson on the second nucleon. The resulting expression for the reaction amplitude represented in Fig. 7 reads

$$T = T^{IA} + T^{IA}\tau_d^0 X_{dd}. \tag{38}$$

Here the scattering amplitude X_{dd} is a solution of the set of equations (31) and (32) taken between ηd configurations, with d being the bound $^3S_1$ NN state. Equation (38), which is formally similar to the well-known distorted wave impulse approximation formula, is the basic expression of our calculation of the $d(\gamma,\pi^0\eta)d$ cross section. An analogous procedure was used for the reaction $^3\text{He}(\gamma,\pi^0\eta)^3\text{He}$.

Following Refs. [19] and [28] we solved the few-body integral equations for ηNN and $\eta - 3N$ only for the lowest s-wave configurations. This approach is well justified by the strong dominance of s waves in the ηN and NN interactions. In Table I we list the values of the ηA scattering length and effective range, which are predicted for three different sets of ηN parameters. As already discussed in the Introduction, there is still no microscopic calculation for the η^4He system, primarily because of the obvious difficulty in the corresponding five-body problem. Therefore, the η-nuclear interaction was taken into account only for the reactions on a deuteron and ^{3}He, whereas for ^{4}He only the absorption of the produced pions was included.

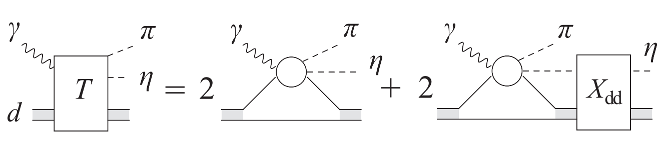

FIG. 7. Representation of the amplitude for $d(\gamma,\pi^0\eta)d$ as given by Eq. (38). In the propagator τ_d in the second term on the right-hand side only the pole contribution τ_d^0 (37) was taken into account.

III. DISCUSSION OF THE RESULTS

We would like to start our discussion with the total cross section presented in Fig. 8. As noted above, its value is independent of the nuclear isospin and should be mostly determined by the spin of the target and its density. In particular, the cross section turns out to be rather sensitive to the details of the target wave function. For example, if one neglects the deuteron d-wave component, the total cross section for $d(\gamma,\pi^0\eta)d$ is reduced by about 30% at $E_\gamma = 1$ GeV with respect to its value obtained with the full deuteron wave function. Furthermore, since, as discussed above, the contributions of the spin-flip and spin-independent parts in $\pi^0\eta$ photoproduction are comparable, the nuclear cross section strongly depends on the nuclear spin. The interplay between the nuclear from factor at high momentum transfer and the spin structure of the production matrix element leads to a nontrivial dependence of the cross section on the choice of the target. As we can see from Fig. 8, without FSI the deuteron cross section turns out to be almost twice as large as that on ^{3}He.

Since for the π-nucleus interaction we take into account only absorption, the only influence of the πA FSI is the attenuation of the cross section. Clearly, it should increase with increasing number of nucleons and increasing nuclear density. This means that among the three nuclei considered here the largest effect should be observed for ^{4}He, as indeed is seen in Fig. 8. Furthermore, absorption is known to be especially important in the region of the $\Delta(1232)$, where the πA scattering becomes highly inelastic, leading for heavier nuclei to the so-called surface production mechanism. In our case it is responsible for a significant reduction of the total cross section, especially above $E_\gamma = 1$ GeV.

As already noted above, an important feature of the reaction (1) is that the time the produced pion spends in the interaction region is short in comparison to that for the η meson. To demonstrate this feature we present in Fig. 9 the distribution of the cross section for $^3\text{He}(\gamma,\pi^0\eta)^3\text{He}$ over the relative velocity in the η^3He and π^3He subsystems. The velocity was calculated in the corresponding ηA and πA c.m. frames as

$$v_{mA} = \frac{\lambda^{1/2}\left(\omega_{mA}^2, M_m^2, M_A^2\right)}{\omega_{mA}^2 - M_m^2 - M_A^2} \tag{39}$$

for $m \in \{\pi,\eta\}$, where the triangle function λ is defined as

$$\lambda(x,y,z) = (x-y-z)^2 - 4yz. \tag{40}$$

As one can see, the maximum in the distribution over $v_{\pi A}$ is shifted to much higher values with respect to the maximum of $d\sigma/dv_{\eta A}$. The corresponding average values of v_{mA} are $v_{\eta A} = 0.38c$ and $v_{\pi A} = 0.83c$.

Using the distribution in Fig. 9 one can estimate the characteristic time the meson m takes to propagate a scattering

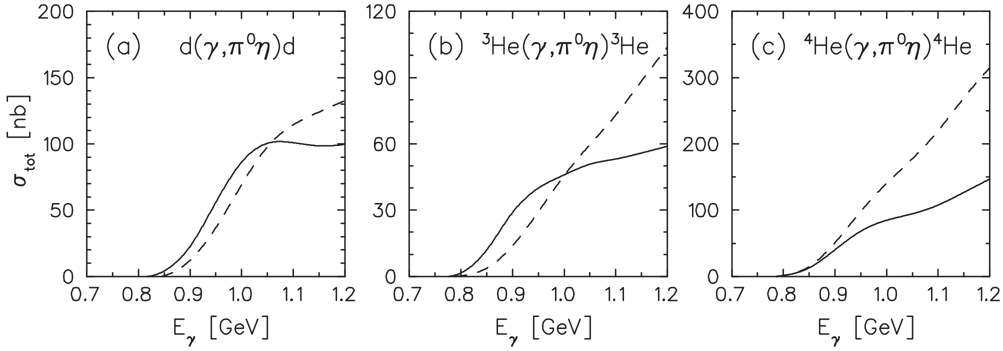

FIG. 8. Total cross section for $\pi^0\eta$ photoproduction on the deuteron, ^{3}He, and ^{4}He. The solid (dashed) curves are obtained with (without) inclusion of the interaction in the final state. For the ηA interaction parameter set 2 in Table I was used. In the case of ^{4}He only pion absorption was taken into account.

center of radius R as

$$t_m = \frac{R + 1/q_m^*}{v_{mA}} + Q_m, \tag{41}$$

where the wavelength $1/q_m^*$ takes into account the wave properties of a particle and Q_m is a time delay due to attraction. Taking $v_{\pi A} = 0.83$ c, $q_\pi^* = 190$ MeV (corresponding to the chosen value of $v_{\pi A}$), $R = 2$ fm, and $Q_\pi = 1/\Gamma_\Delta \approx 1/120\ \text{MeV}^{-1}$ one obtains for the pion $t_\pi \approx 1.62 \times 10^{-23}$ s.

To calculate Q_η one can use the Eisenbud-Wigner formula [60]

$$Q_\eta = 2\frac{d}{dE}\delta_0(E), \tag{42}$$

where $\delta_0(E)$ is the phase shift of the s-wave ηA scattering, for which one can take

$$\delta_0(E) \approx \text{Re}\, a_{\eta A}\sqrt{2\mu_{\eta A}E}. \tag{43}$$

The relative ηA energy E is determined as

$$E = \omega_{\eta A} - M_\eta - M_A, \tag{44}$$

where M_A is the mass of the nucleus. Taking $\text{Re}\, a_{\eta^3He} = 4$ fm from Table I and $E = 38$ MeV (corresponding to the average relative velocity $v_{\eta A} = 0.38c$), one obtains for the time delay

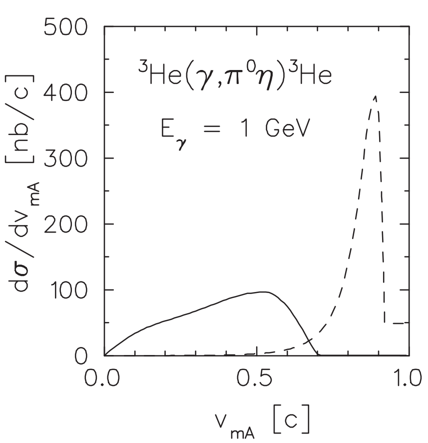

FIG. 9. Distribution of the cross section for $^3\text{He}(\gamma,\pi^0\eta)^3\text{He}$ over the relative velocity in the η^3He (solid curve) and π^3He (dashed curve) subsystems.

$Q_\eta = 6.67 \times 10^{-23}$ s, so that the resulting value of t_η (41) turns out to be 9.34×10^{-23} s, almost six times larger than t_π. This result supports our intuitive assumption that the pion tends to quickly escape the interaction region and its presence should have little effect on the ηA interaction.

To demonstrate the important role of the η-nuclear interaction in our reactions, we show in Figs. 10 and 11 the distribution over the kinetic energy of the η meson in the ηA center-of-mass system. As expected, the spectrum rises rapidly from zero and exhibits a peak very close to the lower limit $T_\eta^* = 0$. On the whole, the inclusion of the ηA FSI enhances the η yield. The resulting total cross in Fig. 8 is visibly increased due to the ηA attraction in the region up to $E_\gamma = 1$ GeV. At higher energies, the pion absorption takes over, leading to the reduction of the total cross section.

As already noted in the previous sections, the interaction of the η meson with the nucleus was included only in the reactions

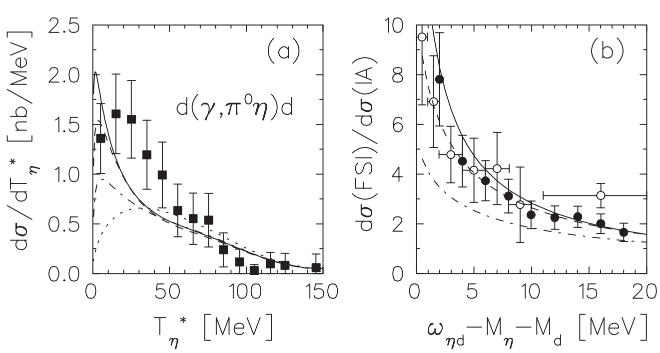

FIG. 10. (a) Kinetic energy spectrum of the η meson in the reaction $d(\gamma,\pi^0\eta)d$ averaged over the energy range $E_\gamma = 0.9$–1.1 GeV. The dotted curve is calculated without the ηd interaction. The dash-dotted, dashed, and the solid curves, including the effect of the ηd interaction, are obtained with sets 1, 2, and 3 of the ηN scattering parameters listed in Table I. In all cases the interaction of the pion with the deuteron is included as described in the text [see Eqs. (12) through (15)]. The filled squares are the preliminary data from Ref. [1]. (b) Ratio of FSI to IA cross sections plotted against the relative ηd energy. Notations of the curves are as on the left panel. Empty and filled circles show the $pn \to \eta d$ and $pd \to \eta pd$ cross sections from Refs. [32] and [33], respectively, divided by the arbitrarily normalized phase space.

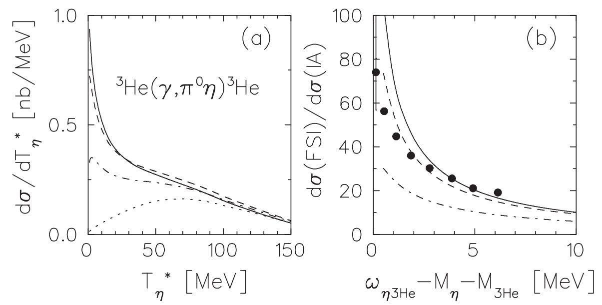

FIG. 11. Same as in Fig. 10 for ^{3}He$(\gamma,\pi^0\eta)^3$He. The points on the right panel show the $pd\to\eta^3$He cross section from Ref. [61] divided by the phase space. The normalization of the data is arbitrary.

on d and ^{3}He, whereas for ^{4}He, where no correct microscopic η^4He model exists, only the absorption of the produced pions was taken into account. In this respect, since the attractive character of the ηA forces leads to a general enhancement of the cross section, the result, shown in Fig. 8(c) by the solid line, is expected to underestimate σ_{tot} at least at low energies.

In the region of low values of the relative ηA momenta $q_\eta^* R \ll 1$, the shape of the spectrum close to the peak may be described in a simple manner as [42,43]

$$\frac{d\sigma}{dE}(E) \sim P(E)\,|f^{(0)}(E)|^2, \tag{45}$$

where $P(E)$ is the reaction phase space and $f^{(0)}(E)$ is the s-wave part of the ηA scattering amplitude, depending on the energy E (44). For ηd elastic scattering $f^{(0)}$ is related to the s-wave part $X_{dd}^{(0)}$ of the matrix X_{dd} in Eqs. (31) and (32) as

$$X_{dd}^{(0)} = -\frac{2\pi}{\mu_{\eta d}} f^{(0)}. \tag{46}$$

Using the effective range formula

$$q_\eta^* \cot\delta_0 = \frac{1}{a} + \frac{r_0}{2} q_\eta^{*2}, \tag{47}$$

one can expand the ratio $P(E)/\sigma(E)$ in powers of the momentum q_η^* as

$$\frac{P(E)}{d\sigma/dE} \sim \frac{1}{|f^{(0)}(E)|^2} = q_\eta^{*2}\,|\cot\delta_0 - i|^2\,, = \sum_{n=0}^{4} C_n q_\eta^{*n}. \tag{48}$$

Since the scattering length $a_{\eta A}$ has a nonzero imaginary part, the expansion (48) contains odd powers of q_η^*. In particular, the ratio of the first two coefficients C_0 and C_1 is proportional to

$$\frac{C_1}{C_0} = -2\,\mathrm{Im}\,a_{\eta A}. \tag{49}$$

The information on the imaginary part of the scattering length is of special interest in the case of the η^3He interaction in view of the existing discrepancy between the theoretical values of a_{η^3He} and the analysis of the measurements of $pd\to\eta^3$He in Refs. [34–36]. According to the latter results, $\mathrm{Im}\,a_{\eta^3He}$ is almost an order of magnitude smaller than $\mathrm{Re}\,a_{\eta^3He}$, being in disagreement with the theoretical predictions of [20,22,26]. Such a strong suppression of the ηN inelasticity in a nucleus is also in contradiction to the intuitive expectation that with an increasing number of nucleons the inelastic effects in the ηA interaction should become more and more important, so that for heavier nuclei the effect of enhancement in the η yield becomes practically invisible [62,63].

Also desirable are measurements of the spectrum in the reaction γ^4He $\to\pi^0\eta^4$He in the region of low η^4He relative energies. As already noted in the Introduction, an enhancement effect due to the η-nuclear attraction, which is rather well seen in the reactions γ^3He $\to\eta^3$He and $pd\to\eta^3$He, was not observed in the reaction $dd\to\eta^4$He [29,30]. It is therefore important to prove whether also the peak in the distribution over the relative energy η^4He in the above reaction will disappear or at least will be much less pronounced in comparison to that observed on d and ^{3}He.

IV. CONCLUSION

In this work we have considered several aspects of the coherent photoproduction of $\pi^0\eta$ pairs on s-shell nuclei. As is discussed in the Introduction, these reactions have some clear advantages, making them preferable to corresponding processes with hadrons as probes. Because of the relative weakness of the electromagnetic interaction, photoinduced reactions are known to furnish a special opportunity to study effects of the interaction in the final state. Furthermore, the underlying elementary process $\gamma N\to\pi^0\eta N$ seems to be under control, in the sense that the results of different analyses [10–12] of the existing data agree with each other. This is in contrast to the reactions $pd\to\eta pd$ or $pd\to\eta^3$He, where the driving mechanism is still not completely understood [31,64,65]. Furthermore, due to smallness of the pion mass the pion tends to escape the interaction region with high velocity, and the major fraction of the production events corresponds to a low relative velocity between η and the recoiling nucleus. This allows one to study in a cleaner way the η-nuclear interaction in comparison to $pd\to\eta pd$, where the pd interaction in the final state should always strongly affect the interaction between the η meson and the deuteron. Therefore, measurements of these reactions may be an additional important source of information on the ηN low-energy dynamics.

One of the innovations of the present paper is the study of the dependence of the total cross section on the spin and isotopic spin of the target. Since the $\pi^0\eta$ photoproduction seems to be dominated by the D_{33} wave, among the s-shell nuclei the largest cross section is predicted for ^{4}He, whereas for ^{3}He it appears to be half of that for the deuteron.

We have analyzed the effects of the final state interaction in the region of low ηA relative energies. In the simplest case when the pole in the amplitude is close to zero energy, a measurement of the distribution over the relative ηA energy may be utilized to estimate the relative value of the imaginary part of the scattering length $a_{\eta A}$ using the ratio (49) of the first two coefficients in the polynomial ansatz (48). This information is clearly important for our understanding of the role of inelasticity in the ηA interaction at low energy.

It is also worth mentioning that coherent $\pi^0\eta$ photoproduction on ^{4}He provides a unique opportunity to obtain information on the $\eta\,^4$He interaction in electromagnetic processes on ^{4}He. By contrast, in the reaction $^4\mathrm{He}(\gamma,\eta)^4\mathrm{He}$, where the s wave in the final state is forbidden by the spin-selection rule, the cross section appears to be practically insensitive to the $\eta\,^4$He interaction effect.

ACKNOWLEDGMENTS

Valuable discussions with Christoph Hanhart are much appreciated. We also acknowledge support from the Dynasty Foundation, MSE Program "Nauka," RFBR Grant No. 12-02-00560-a, as well as from the Tomsk Polytechnic University.

[1] B. Krusche, Eur. Phys. J.: Spec. Top. **198**, 199 (2011).
[2] T. Nakabayashi *et al.*, Phys. Rev. C **74**, 035202 (2006).
[3] J. Ajaka *et al.*, Phys. Rev. Lett. **100**, 052003 (2008).
[4] I. Horn *et al.* (CB-ELSA Collaboration), Phys. Rev. Lett. **101**, 202002 (2008).
[5] V. L. Kashevarov *et al.* (Crystal Ball at MAMI and TAPS and A2 Collaborations), Eur. Phys. J. A **42**, 141 (2009).
[6] E. Gutz *et al.* (CB-ELSA Collaboration), Eur. Phys. J. A **35**, 291 (2008).
[7] E. Gutz *et al.* (CB-ELSA and TAPS Collaborations), Phys. Lett. B **687**, 11 (2010).
[8] E. Gutz (CBELSA-TAPS Collaboration), AIP Conf. Proc. **1257**, 581 (2010).
[9] V. L. Kashevarov *et al.* (Crystal Ball at MAMI, TAPS, and A2 and TAPS and A2 Collaborations), Phys. Lett. B **693**, 551 (2010).
[10] M. Doring, E. Oset, and D. Strottman, Phys. Rev. C **73**, 045209 (2006).
[11] I. Horn *et al.*, Eur. Phys. J. A **38**, 173 (2008).
[12] A. Fix, V. L. Kashevarov, A. Lee, and M. Ostrick, Phys. Rev. C **82**, 035207 (2010).
[13] M. Döring, E. Oset, and U.-G. Meissner, Eur. Phys. J. A **46**, 315 (2010).
[14] J. Beringer *et al.* (Particle Data Group), Phys. Rev. D **86**, 010001 (2012).
[15] N. V. Shevchenko, S. A. Rakityansky, S. A. Sofianos, V. B. Belyaev, and W. Sandhas, Phys. Rev. C **58**, R3055 (1998).
[16] A. Deloff, Phys. Rev. C **61**, 024004 (2000).
[17] H. Garcilazo and M. T. Pena, Phys. Rev. C **61**, 064010 (2000).
[18] S. Wycech and A. M. Green, Phys. Rev. C **64**, 045206 (2001).
[19] A. Fix and H. Arenhövel, Nucl. Phys. A **697**, 277 (2002).
[20] A. Fix and H. Arenhövel, Phys. Rev. C **66**, 024002 (2002).
[21] A. Fix and H. Arenhövel, Phys. Lett. B **492**, 32 (2000).
[22] N. V. Shevchenko, V. B. Belyaev, S. A. Rakityansky, S. A. Sofianos, and W. Sandhas, Nucl. Phys. A **689**, 383 (2001).
[23] H. Garcilazo and M. T. Pena, Phys. Rev. C **66**, 034606 (2002).
[24] A. Fix and H. Arenhövel, Eur. Phys. J. A **19**, 275 (2004).
[25] N. J. Upadhyay, K. P. Khemchandani, B. K. Jain, and N. G. Kelkar, Phys. Rev. C **75**, 054002 (2007).
[26] S. Wycech, A. M. Green, and J. A. Niskanen, Phys. Rev. C **52**, 544 (1995).
[27] N. V. Shevchenko, V. B. Belyaev, S. A. Rakityansky, S. A. Sofianos, and W. Sandhas, Nucl. Phys. A **699**, 165 (2002).
[28] A. Fix and H. Arenhövel, Phys. Rev. C **68**, 044002 (2003).
[29] R. Frascaria *et al.*, Phys. Rev. C **50**, R537 (1994).
[30] P. Adlarson *et al.* (WASA-at-COSY Collaboration), Phys. Rev. C **87**, 035204 (2013).
[31] J. F. Germond and C. Wilkin, J. Phys. G **15**, 437 (1989).
[32] H. Calen *et al.*, Phys. Rev. Lett. **79**, 2642 (1997).
[33] R. Bilger *et al.*, Phys. Rev. C **69**, 014003 (2004).
[34] J. Smyrski *et al.*, Phys. Lett. B **649**, 258 (2007).
[35] H.-H. Adam *et al.*, Phys. Rev. C **75**, 014004 (2007).
[36] T. Mersmann *et al.*, Phys. Rev. Lett. **98**, 242301 (2007).
[37] F. Pheron *et al.*, Phys. Lett. B **709**, 21 (2012).
[38] W. Krzemien, P. Moskal, J. Smyrski, and M. Skurzok, EPJ Web Conf. **37**, 02003 (2012).
[39] V. A. Baskov *et al.*, arXiv:1212.6313 [nucl-ex].
[40] C. Wilkin *et al.*, Phys. Lett. B **654**, 92 (2007).
[41] J. A. Niskanen and H. Machner, Nucl. Phys. A **902**, 40 (2013).
[42] K. M. Watson, Phys. Rev. **88**, 1163 (1952).
[43] A. B. Migdal, Sov. Phys. JETP **1**, 2 (1955); see also *Qualitative Methods in Quantum Theory* (Perseus, Cambridge, MA, 2000).
[44] R. Machleidt, K. Holinde, and C. Elster, Phys. Rep. **149**, 1 (1987).
[45] V. Baru, J. Haidenbauer, C. Hanhart, and J. A. Niskanen, Eur. Phys. J. A **16**, 437 (2003).
[46] H. S. Sherif, M. S. Abdelmonem, and R. S. Sloboda, Phys. Rev. C **27**, 2759 (1983).
[47] C. Lazard and Z. Maric, Nuovo Cimento A **16**, 605 (1973).
[48] C. B. Dover and S. N. Yang, Phys. Lett. B **50**, 217 (1974).
[49] S. Fernbach, R. Serber, and T. B. Taylor, Phys. Rev. **75**, 1352 (1949).
[50] R. M. Frank, J. L. Gammel, and K. M. Watson, Phys. Rev. **101**, 891 (1956).
[51] C. A. Engelbrecht, Phys. Rev. **133**, B988 (1964).
[52] D. Drechsel, S. S. Kamalov, and L. Tiator, Eur. Phys. J. A **34**, 69 (2007).
[53] B. Krusche *et al.*, Eur. Phys. J. A **6**, 309 (1999).
[54] F. Rambo *et al.*, Nucl. Phys. A **660**, 69 (1999).
[55] H. Zankel, W. Plessas, and J. Haidenbauer, Phys. Rev. C **28**, 538 (1983).
[56] C. Wilkin, Phys. Rev. C **47**, R938 (1993).
[57] A. M. Green and S. Wycech, Phys. Rev. C **55**, R2167 (1997).
[58] R. A. Arndt, W. J. Briscoe, T. W. Morrison, I. I. Strakovsky, R. L. Workman, and A. B. Gridnev, Phys. Rev. C **72**, 045202 (2005).
[59] A. S. Rinat and A. W. Thomas, Nucl. Phys. A **282**, 365 (1977).
[60] E. P. Wigner, Phys. Rev. **98**, 145 (1955).
[61] B. Mayer *et al.*, Phys. Rev. C **53**, 2068 (1996).
[62] H. C. Chiang, E. Oset, and L. C. Liu, Phys. Rev. C **44**, 738 (1991).
[63] Y. Maghrbi *et al.*, Eur. Phys. J. A **49**, 38 (2013).
[64] U. Tengblad, G. Faldt, and C. Wilkin, Eur. Phys. J. A **25**, 267 (2005).
[65] Y. N. Uzikov, Nucl. Phys. A **801**, 114 (2008).